UCRL-TB-136037

Preliminary Report: Dosimetric Accuracy of the PEREGRINE™ Dose Calculation System

C.L. Hartman Siantar, R.S. Walling, R.W. Patterson, S.H. May, R.K. House, D.K. Knapp, D. Williams, T.P. Daly, D. Garrett, C. Powell, D. Jong

October 22, 1999

U.S. Department of Energy

Lawrence Livermore National Laboratory

DISCLAIMER

Work performed under the auspices of the U. S. Department of Energy by the University of California Lawrence Livermore National Laboratory under Contract W-7405-Eng-48.

Preliminary Report:
Dosimetric Accuracy of the
PEREGRINE™ Dose Calculation System

Lawrence Livermore National Laboratory

October 22, 1999

Preliminary Report:
Dosimetric Accuracy of the PEREGRINE™ Dose Calculation System

Introduction

Monte Carlo methods are described as a gold standard for three-dimensional radiation therapy dose calculations because they accurately compute dose in a wide variety of radiation therapy conditions.[1 2 3] Recent comparisons of dose distributions calculated using Monte Carlo vs. conventional methods indicate surprising differences for several tumor sites.[4 5 6]

To calculate dose for radiation therapy, a Monte Carlo code simulates the transport of hundreds of millions of photons, electrons and positrons through a three-dimensional computer model of the beam delivery system and patient. The beam delivery system is described from accelerator manufacturer specifications, while the patient is described from a treatment-planning CT scan.

The PEREGRINE™ system implements the Monte Carlo method for the specific purpose of simulating radiotherapy treatments. The major goals in its development have been to design a system specifically tailored to radiation therapy applications and make Monte Carlo transport fast enough to be practical for day-to-day treatment planning. Operating in a multi-cpu environment consisting of low-cost, commodity hardware, PEREGRINE™ enables real time visualization of dose as it is simulated, and completes a full treatment simulation in minutes.[7 8 9]

To verify the dosimetric accuracy of PEREGRINE™ dose calculations, we developed a comprehensive suite of ion chamber and diode measurements with standard clinical photon beams incident on numerous patient-substitute phantoms. The tests are designed to answer two basic questions: "Does the method represent the radiation source with sufficient accuracy to result in accurate dose calculations?" and "Are the Monte Carlo data and algorithms, used to track particles through the system, sufficient to accurately predict dose in the patient?"

In the set of comparisons presented here, we demonstrate PEREGRINE's accuracy for a wide range of beam and patient configurations using a manufacturer's general description of a clinical accelerator. These conditions test all the important Monte Carlo transport algorithms. We find that PEREGRINE™ accuracy is consistent with both the ICRU 42[10] recommendations and also significantly smaller than the experience-based criteria given in AAPM Task Group 53 Report.[11] Because of its speed and ease of use, PEREGRINE™ has the near-term ability to bring Monte Carlo radiation transport calculations to the RTP desktop environment.

Materials and Methods

To design the verification program, we examined the basic characteristics of the Monte Carlo approach and the general functionality and assumptions of the PEREGRINE™ system. We combined the results of that examination with

recommendations from AAPM TG 53 and other references.[12] [13] This combination of existing standards plus Monte Carlo specific considerations results in a test suite that covers a broad range of radiation device and patient configurations found in the clinic. We then employ this test suite to assess the accuracy of the PEREGRINE™ system against a set of dosimetric accuracy standards.

Characteristics of the PEREGRINE™ Monte Carlo Dose Calculation System

The PEREGRINE™ dose calculation system is described in detail elsewhere.[7] [8] [9] PEREGRINE™ simulates radiation therapy starting with a set of representative particles randomly sampled from energy, angle, and position distributions determined from offline simulations of the treatment-independent portion of the radiation source. It then tracks each photon, electron, and positron through the treatment-dependent beam delivery system and through the patient using standard Monte Carlo transport methods. As each particle interacts, it sets in motion other particles that are also tracked. Photons and electrons are tracked to a minimum energy of 1 and 10 keV, respectively. The minimum energy for delta ray and bremsstrahlung production is 200 keV.

Treatment-specific beam modifiers such as collimator jaws, apertures, blocks, multileaf collimators and wedges are modeled explicitly during each PEREGRINE™ calculation. Each component is described in terms of its physical dimensions, material composition, and density.

The patient or phantom is described as a Cartesian map of material composition and density determined from the patient's CT scan. Each CT pixel defines the atomic composition and density of a corresponding transport mesh voxel. Material composition is determined from user-defined CT threshold values. Density is determined from a user-defined piecewise-linear function that describes the CT-number-to-density conversion.

PEREGRINE™ records the dose deposited by each particle in a uniform Cartesian dose collection mesh that consists of packed dose-collection spheres.

The on-site instantiation process for PEREGRINE™ involves selection of the appropriate accelerator make/model from an online library, calibration in terms of Gray per monitor unit based on the calibration conditions used on-site, and +/- 10% tuning of the energy of the electron beam incident on the photon-conversion target.

Once this process is complete, PEREGRINE™ calculates absolute dose per monitor unit for all beam configurations, with no additional empirical corrections.

Test Suite Description

While developing a comprehensive dosimetric verification test suite, we reviewed recommendations proposed by Van Dyk[12], Fraass[13], and the TG 53 Report[11], selecting a set of measurements that stress the special capabilities provided by Monte Carlo simulation. Two basic features were tested: characterization of the radiation source and photon and electron transport in both the beam delivery system and patient. The test suite is summarized in Table 1.

Accurate characterization of the treatment-independent portion of the beam delivery system, including the electron beam, photon-conversion target, primary collimator, flattening filter, *etc.*, establishes the basic characteristics of the radiation source. Previous work[14] has already demonstrated that the source-characterization method of condensing the description of the radiation source into a primary subsource plus several scatter

Table 1.Test suite summary.

Test Category	Tests	Measurement Description
Open Fields	**Square Fields** 2x2, 5x5, 10x10, 20x20, 38x38 cm	Depth dose Inplane and crossplane profiles at depths of 5, 10, 20 cm (6 MV) and 10, 20, 30 cm (18 MV)
	Rectangular Fields 20x5, 5x20, 40x5, 5x40 cm	Depth dose
	Off-axis Fields 10x10 cm, jaw at central axis; 5x5 cm, center of field 10 cm off central axis	Depth dose
	Blocks 20x20 cm field with quarter-beam block, half-beam block, half-beam block with 50% transmission, and 2x8 cm central block	Depth dose 5 cm off-axis for half-beam blocks, 7.5 cm off-axis for quarter-beam block Crossplane profiles at depths of 5, 10, 20 cm (6 MV) and 10, 20, 30 cm (18 MV)
Beam Modifiers	**Wedges** 15°, 45°, 60° wedges with largest field size for each wedge	Depth dose Crossplane profiles at depths of 5, 10, 20 cm (6 MV) and 10, 20, 30 cm (18 MV)
	Compensator Step compensator with (x, x, x, x% transmission steps)	Crossplane profiles at depths of 5, 10, 20 cm (6 MV) and 10, 20, 30 cm (18 MV)
	Multileaf Collimator Variable-spaced leaf comb pattern	Crossplane profiles at depths of 1, 5, 10, 20 cm (6 MV) and 3.2, 10, 20, 30 cm (18 MV)
Irregular Surface	Lucite hemisphere on water surface	Crossplane profiles at depths of 5, 10, 20 cm (6 MV) and 10, 20, 30 cm (18 MV)
	2 cm step on water surface	Crossplane profiles at depths of 1, 5, 10, 20 cm (6 MV) and 1, 3, 10, 20, 30 cm (18 MV)
Heterogeneities	2 cm air half-slab	Depth dose 5 cm off-axis on water-only and water-heterogeneity side field Profiles 5, 10, 20 cm (6 MV) and 5, 10, 20, 30 cm below bottom surface of heterogeneity
	2 cm lung-equivalent half-slab	
	2 cm bone-equivalent half-slab	
	2 cm iron half-slab	

subsources, characterized in terms of radially-dependent energy and angular distributions accurately reproduces the original energy and angular distributions exiting the accelerator head. Our dosimetric comparisons demonstrate that this method results in accurate prediction of absolute dose per monitor unit.

The simplest and most direct radiation source tests are open fields incident on water phantoms: depth dose for small to large fields, field flatness or horns for large fields, and relative output for small, large, and high aspect-ratio (rectangular) fields. In addition, depth dose comparisons for independent-jaw fields tests the adequacy of off-axis photon energy distributions.

Once the radiation source is established, PEREGRINE™ uses accurate, efficient Monte Carlo methods to transport photons, electrons, and positrons through the patient-dependent beam delivery system (including the air) and the patient.

Accurate photon particle-interaction data and transport algorithms are critical for determining relative attenuation and scatter in accelerator-head components, beam modifiers, and the patient. Their accuracy affects calculated dose distribution's depth-dose, field flatness and relative output, and are most directly assessed in regions of transient charged particle equilibrium. The verification program described here tests photon transport algorithms in PEREGRINE™ in three ways:

- By experimentally verifying the water-phantom dose distributions resulting from beam modifiers such as blocks, block trays, wedges, multileaf collimators, and compensators, we assess the accuracy of photon attenuation and scatter in high- and low-atomic number materials outside the patient or phantom
- By experimentally verifying dose distributions in phantoms with step (discontinuous) and partial-cylinder (continuously changing) surface irregularities, we assess the accuracy of photon attenuation and scatter inside a water/water-equivalent phantom
- By experimentally verifying dose distributions in phantoms with internal heterogeneities, we assess the accuracy of photon and attenuation inside the phantom in the presence of heterogeneities with high- and low-atomic number and high- and low-density

Accurate electron and positron transport is most important in regions of electron disequilibrium. These regions are located less than one electron range from a significant material boundary, such as the outer surface of the phantom or internal-heterogeneity surfaces. The dose predicted in the dose-buildup region near the initial patient or phantom surface depends on accurate electron transport for two reasons. First, dose is contributed directly by contaminant electrons produced in the beam delivery system and the air. Second, dose is contributed from electrons created by photon interactions in the patient or phantom (this is also an electronic disequilibrium area).

Finally, modeling (or not modeling) the electron scatter into the monitor chamber may contribute to uncertainty in relative dose predictions. PEREGRINE™ does not predict backscatter into the monitor chamber; instead, it uses published collimator jaw-dependent backscatter measurements[15] to estimate this correction to the absolute output per monitor unit. The accuracy of this approach is assessed in the beam delivery system tests.

We test PEREGRINE's electron/positron transport algorithms by experimentally verifying dose near internal heterogeneity interfaces. This demonstrates the accurate electron transport around heterogeneities with high- and low-atomic number and high- and low-density.

Measurements

Water phantom measurements were made at the University of California San Francisco. Output, profile and depth dose measurements were made using a Wellhofer IC-10 ionization chamber (0.14 cm^3 active volume with a 6 mm diameter and 3.3 mm active length, 0.4 cm wall thickness) in a Wellhofer water phantom system.

Diode measurements are reported for the 2x2 profile and heterogeneity measurements because of their superior spatial resolution. Measurements were made at University of California San Francisco Department of Radiation Oncology with a Scanditronix photon diode, ID # FP1329 1990 (p-type silicon, chip thickness of 0.45 mm, 2.5 mm diameter) in a Wellhofer water phantom system. Diode measurements are corrected to match Markus ion chamber measurements (2 mm thick, 6 mm diameter cylindrical collection volume) in regions of transient electronic equilibrium. This correction was determined by averaging the correction determined at 5 cm off-axis, on both the water and heterogeneity side of the phantom.

Figure 1. Experimental configurations for step surface (A), partial-cylinder phantoms (B and C), and half-slab heterogeneity phantoms (D).

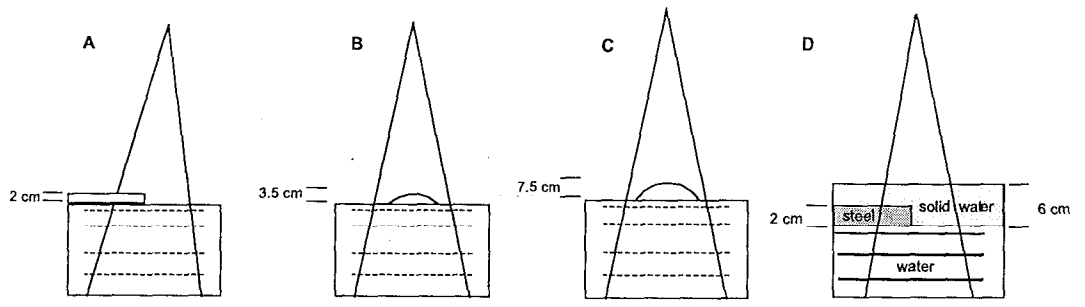

Measurements were made at a source-to-surface distance (SSD) of 90 cm. This distance was chosen to be representative of typical clinical configurations. Calculations used Monte Carlo simulations of 6 MV and 18 MV beams from the Varian Clinac 2100C linear accelerator. Beams were calibrated to produce 1 cGy/MU at 1.5 cm / 3.5 cm depth (6 / 18 MV beam) and 100 cm SSD in water for a 10x10 cm field.

Calculations

All calculations are reported in absolute dose per monitor unit. The 6 and 18 MV nominal energy beams were simulated from manufacturer-specified Varian 2100C materials and dimensions. 6.2 and 18.5 MeV incident electron beams were used in the simulation calculations for the 6 and 18 MV beams, respectively. The only empirical factor applied to the Monte Carlo calculations shown here was the calibration to Gy-to-monitor units for a 10x10 cm field. PEREGRINE™ calculations were run for a sufficient amount of time to have a statistical uncertainty of less than or equal to 0.5% of the maximum dose.

Accuracy Standards and Metrics

Dosimetric accuracy required for treatment planning has been the subject of much discussion. Cunningham[16] suggests that an overall accuracy of 5% in dose delivery may be possible with achievable uncertainties of 2.5% in beam calibration, 3-4% in dose calculations, and 3-4% in treatment delivery.

Cunningham's goal of better than 4% uncertainty in treatment planning dose calculations may be compared with more detailed recommendations on dose calculation accuracy. These recommendations are generally divided into acceptable limits for high and low dose gradient areas. Van Dyk *et al.*[12] described "Criteria for Acceptability" for a series of dosimetric situations. Their method of accuracy characterization in terms of

areas of the beam and treatment configurations is also supported by TG 53[11], which divides the radiation beam into a central, high-dose portion, a penumbral region, an outside region, a buildup region, and central axis, and a normalization point. Different accuracy acceptability criteria, ranging from 0.5% to 50% of the central ray normalization dose, are assigned to various regions of the beam. These suggested criteria are based on collective expectations of members of the task group for the prevailing dose calculation methods in clinical use at that time (1996).

ICRU 42[10] recommended an accuracy goal of 2% and 2 mm, however it was not considered attainable with current clinically-implemented dose calculation methods.

Monte Carlo methods should be able to achieve the ICRU 42[10] goal of 2% and 2 mm accuracy for low- and high-dose-gradient regions, including the buildup region. Combined with a 2% statistical standard deviation in dose, this performance should still result in a total uncertainty of less than 3%, in conformance with Cunningham's overall accuracy goal, which was based on radiobiological grounds.

To succinctly describe the agreement between the numerous calculation-measurement comparisons, we developed a two-part figure of merit that emphasizes fractional dose error in homogeneous-dose regions and positional error in high dose-gradient regions. High- and low-gradient regions are identified using a generalized second-difference method, optimized to detect peaks in the first derivative with a characteristic width.

The fractional dose error ΔD is defined as:

$$\Delta D(x) = \frac{(D_C(x) - D_T(x))}{D_{C\,ref}},$$

where $D_C(x)$ and $D_T(x)$ are the calculated and true doses at point x, and D_{Cref} is a reference calculated dose; we use $D_{Cref} = D_{Cmax}$, the maximum calculated dose in the patient volume.

The position error Δx is defined as:

$$\Delta x = \begin{cases} x - x_C \ni D_C(x_C) = D_T(x), & D_T(x) < D_C(x) \\ -(x - x_T) \ni D_T(x_T) = D_C(x), & D_T(x) > D_C(x) \end{cases},$$

where $D_C(x)$ and $D_T(x)$ are the calculated and true doses at point x. In the first case, Δx is the distance from a given point x to the point x_C at which $D_C(x_C) = D_T(x)$; in the second, it is the distance from point x to the point x_T at which $D_T(x_T) = D_C(x)$.

As figures of merit, we use the RMS values of ΔD and Δx:

$$\langle \Delta D \rangle_{RMS} = \sqrt{\sum_{x \in \Delta D} (\Delta D)^2}$$

and $$\langle \Delta x \rangle_{RMS} = \sqrt{\sum_{x \in \Delta x} (\Delta x)^2}.$$

Results

Comparisons of PEREGRINE™ calculations with dosimetric measurements for clinical radiation therapy beams demonstrate the ability of three-dimensional Monte Carlo methods to accurately model a wide variety of radiation source configurations and

predict dose in both homogeneous and heterogeneous media. We have compared the results of measurements and PEREGRINE™ calculations for all cases described in Table 1. Tables 2-4 summarize the agreement between measurements and calculations by stating the RMS average error in percent of the maximum dose for low-dose-gradient regions and RMS average error in mm for high dose-gradient regions. Results demonstrate the excellent agreement between calculations and measurements. In all cases, the RMS difference between measurements and calculations is less than the ICRU goal of 2%.

Results for square, rectangular, and asymmetric open fields indicate excellent agreement between experiments and measurements. RMS relative-dose and position deviations are summarized in Table 2. These tests, including depth dose for small to large fields, field flatness or horns for large fields, relative output for small, large, and high aspect-ratio (rectangular) fields, and off-axis depth dose comparisons for asymmetric fields, provide the simplest, most direct test of the radiation source.

Figures 2-4 demonstrate the accuracy of the PEREGRINE™ source model for predicting depth dose, field flatness, penumbra, and absolute output. Figure 2 compares PEREGRINE™ calculations with central axis depth dose measurements for symmetric square fields. PEREGRINE™ accurately reproduces the absolute dose per monitor unit, as well as the change in depth dose as a function of field size. For all 6 MV fields and 18 MV field sizes of 5x5 cm or greater, the slope of the depth dose curve decreases with increasing field size. This is due to the influence of phantom-scattered photons on the dose at depth. The 18 MV 2x2 cm field shows a substantially smaller slope, due to the additional effects of electron transport out of the narrow beam.

Figure 3 demonstrates profile comparisons for 2x2 to 38x38 cm fields, measured at 5 cm and 10 cm depth for 6-MV and 18-MV beams, respectively. Results highlight PEREGRINE's ability to accurately reproduce field flatness, as demonstrated by the largest fields, and beam fall-off, primarily as demonstrated by the smallest fields. Correct prediction of field flatness for the largest fields requires accurate simulation of both fluence and photon energy, both of which vary rapidly as a function of off-axis distance. For the smallest fields, the profile shape is affected by electron transport out of the beam, especially for 18 MV.

Taken together, measurement comparisons for these open field calculations provide substantial evidence supporting the claim that PEREGRINE's source model accurately simulates the treatment-independent beam delivery system.

Table 2. Open field comparisons

Description	Data type	6 MV			18 MV			Detector
		Location	Accuracy	Position	Location	Accuracy	Position	
2x2 cm	DepthDose	central axis	1.13 %	N/A	central axis	1.04 %	N/A	IC-10
	XProfile	depth=5cm	1.11 %	0.40 mm	depth=10cm	0.47 %	0.33 mm	Diode
	XProfile	depth=10cm	1.38 %	0.48 mm	depth=20cm	1.36 %	0.53 mm	Diode
	XProfile	depth=20cm	0.38 %	0.43 mm	depth=30cm	1.35 %	0.40 mm	Diode
	YProfile	depth=5cm	1.75 %	0.99 mm	depth=10cm	1.43 %	0.91 mm	Diode
	YProfile	depth=10cm	1.37 %	1.05 mm	depth=20cm	1.46 %	1.21 mm	Diode
	YProfile	depth=20cm	0.31 %	1.28 mm	depth=30cm	1.07 %	1.25 mm	Diode
5x5 cm	DepthDose	central axis	0.91 %	N/A	central axis	0.64 %	N/A	IC-10
	XProfile	depth=5cm	1.55 %	0.74 mm	depth=10cm	0.76 %	0.43 mm	IC-10
	XProfile	depth=10cm	1.00 %	0.66 mm	depth=20cm	0.40 %	0.44 mm	IC-10
	XProfile	depth=20cm	0.30 %	0.58 mm	depth=30cm	0.58 %	0.39 mm	IC-10
	YProfile	depth=5cm	1.27 %	0.92 mm	depth=10cm	0.41 %	0.46 mm	IC-10
	YProfile	depth=10cm	0.96 %	0.63 mm	depth=20cm	0.46 %	0.41 mm	IC-10
	YProfile	depth=20cm	0.21 %	0.49 mm	depth=30cm	0.61 %	0.61 mm	IC-10
10x10 cm	DepthDose	central axis	0.42 %	N/A	central axis	0.62 %	N/A	IC-10
	XProfile	depth=5cm	0.66 %	0.61 mm	depth=10cm	0.58 %	0.41 mm	IC-10
	XProfile	depth=10cm	0.44 %	0.70 mm	depth=20cm	0.37 %	0.39 mm	IC-10
	XProfile	depth=20cm	0.30 %	0.55 mm	depth=30cm	0.44 %	0.41 mm	IC-10
	YProfile	depth=5cm	0.60 %	0.66 mm	depth=10cm	0.47 %	1.01 mm	IC-10
	YProfile	depth=10cm	0.46 %	1.16 mm	depth=20cm	0.40 %	0.86 mm	IC-10
	YProfile	depth=20cm	0.35 %	0.72 mm	depth=30cm	0.49 %	0.91 mm	IC-10
20x20 cm	DepthDose	central axis	0.54 %	N/A	central axis	0.34 %	N/A	IC-10
	XProfile	depth=5cm	1.35 %	0.44 mm	depth=10cm	0.52 %	0.48 mm	IC-10
	XProfile	depth=10cm	0.56 %	0.38 mm	depth=20cm	0.33 %	0.28 mm	IC-10
	XProfile	depth=20cm	0.71 %	0.37 mm	depth=30cm	0.35 %	0.18 mm	IC-10
	YProfile	depth=5cm	1.36 %	0.89 mm	depth=10cm	0.73 %	1.15 mm	IC-10
	YProfile	depth=10cm	0.58 %	1.33 mm	depth=20cm	0.51 %	0.69 mm	IC-10
	YProfile	depth=20cm	0.70 %	0.82 mm	depth=30cm	0.35 %	0.78 mm	IC-10
38x38 cm	DepthDose	central axis	0.74 %	N/A	central axis	0.30 %	N/A	IC-10
	XProfile	depth=5cm	1.80 %	0.34 mm	depth=10cm	0.59 %	0.29 mm	IC-10
	XProfile	depth=10cm	1.44 %	0.36 mm	depth=20cm	0.36 %	0.32 mm	IC-10
	XProfile	depth=20cm	0.94 %	0.36 mm	depth=30cm	0.41 %	0.30 mm	IC-10
5x20 cm	DepthDose	central axis	0.85 %	N/A	central axis	0.57 %	N/A	IC-10
20x5 cm	DepthDose	central axis	0.62 %	N/A	central axis	0.61 %	N/A	IC-10
5x40 cm	DepthDose	central axis	0.37 %	N/A	central axis	0.99 %	N/A	IC-10
40x5 cm	DepthDose	central axis	0.41 %	N/A	central axis	0.86 %	N/A	IC-10
5x5 10 cm Off-Axis	DepthDose	at Y= -10 cm	0.52 %	N/A	at Y= -10 cm	0.42 %	N/A	IC-10
10x10 5 cm Off-Axis	DepthDose	at X=5 cm	0.44 %	N/A	at X=5 cm	0.50 %	N/A	IC-10

Figure 2. Dose profiles for 2, 5, 10, 20, and 38 cm square fields.

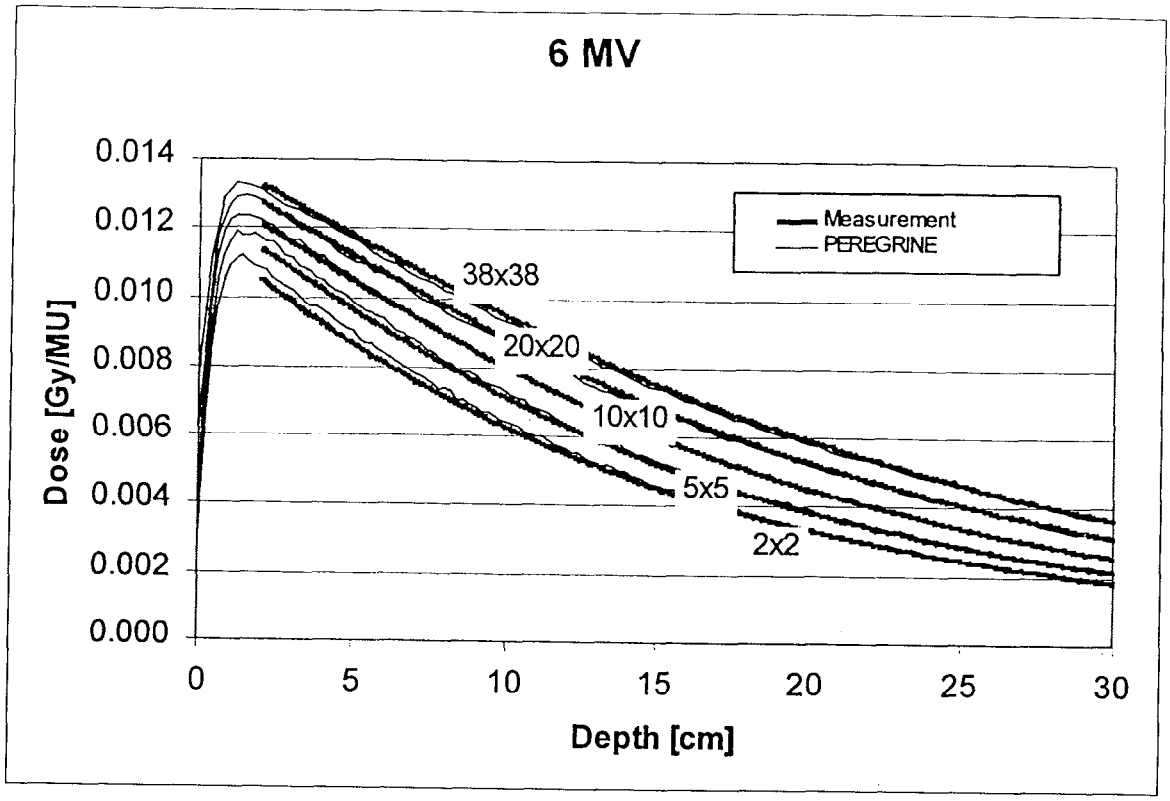

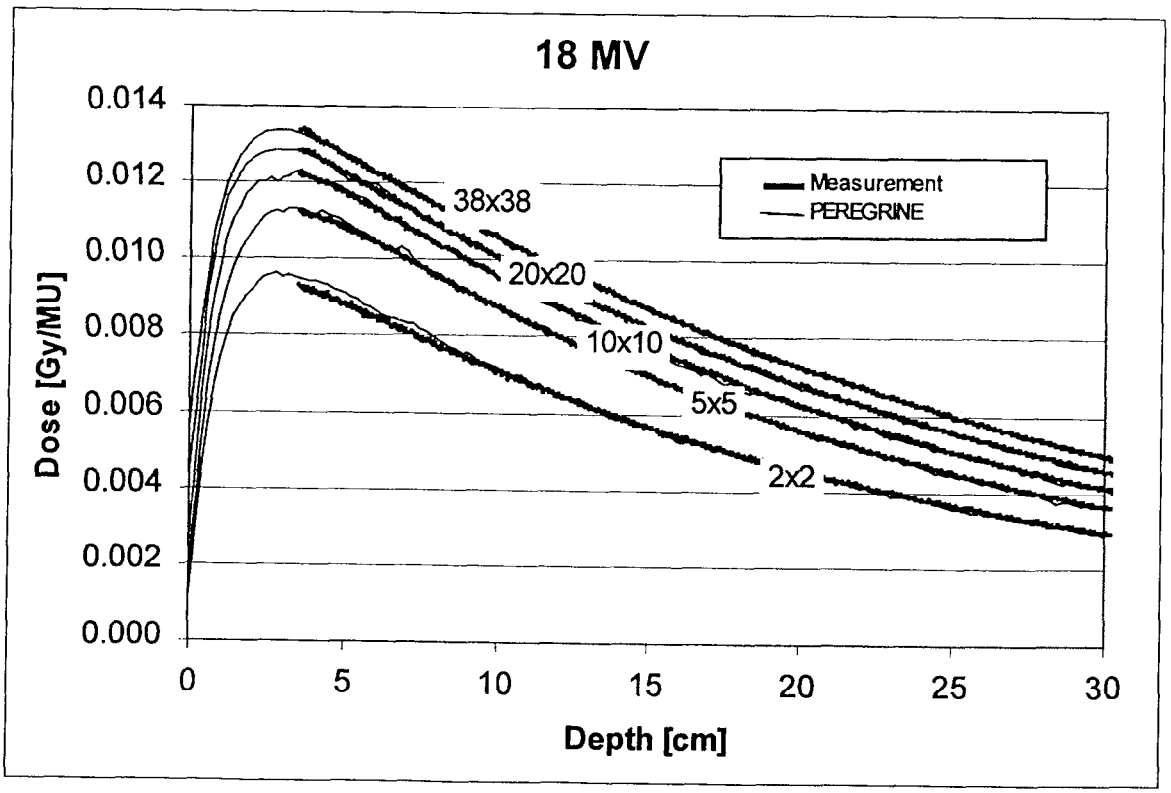

Figure 3. Profile dose distributions for 2, 5, 10, 20, and 38 cm square fields.

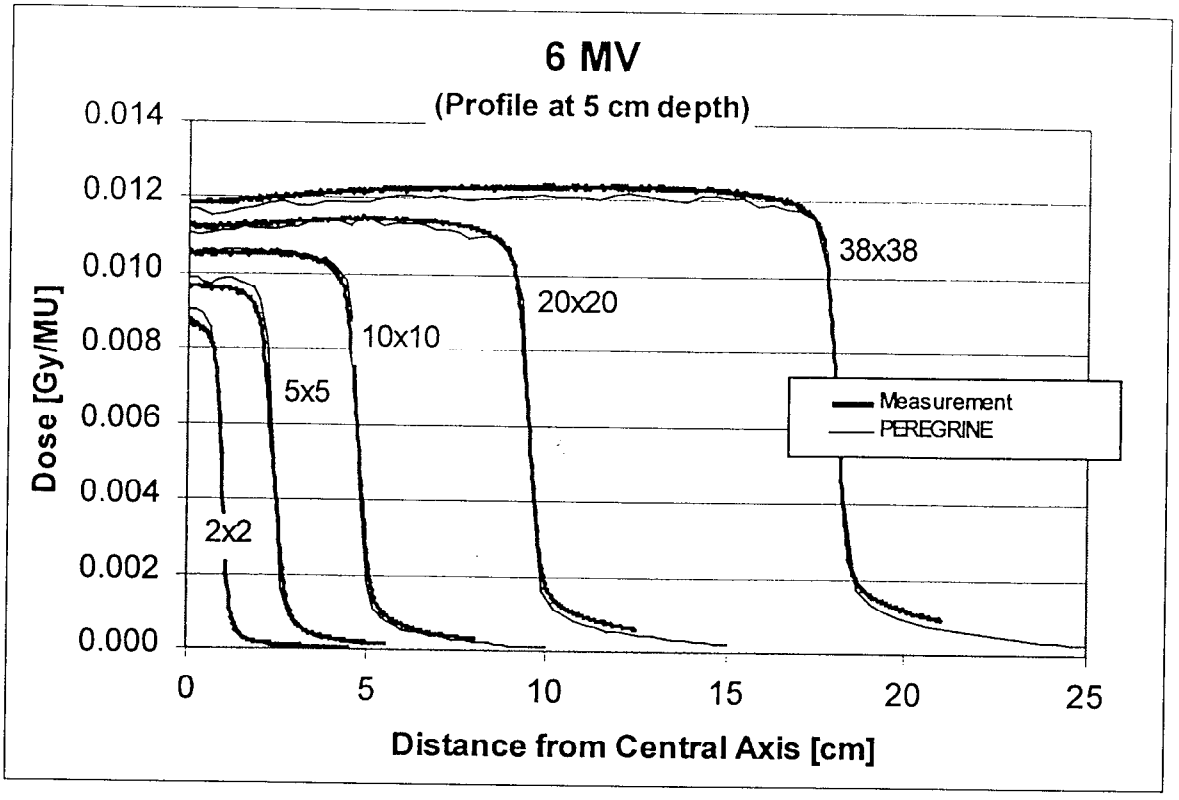

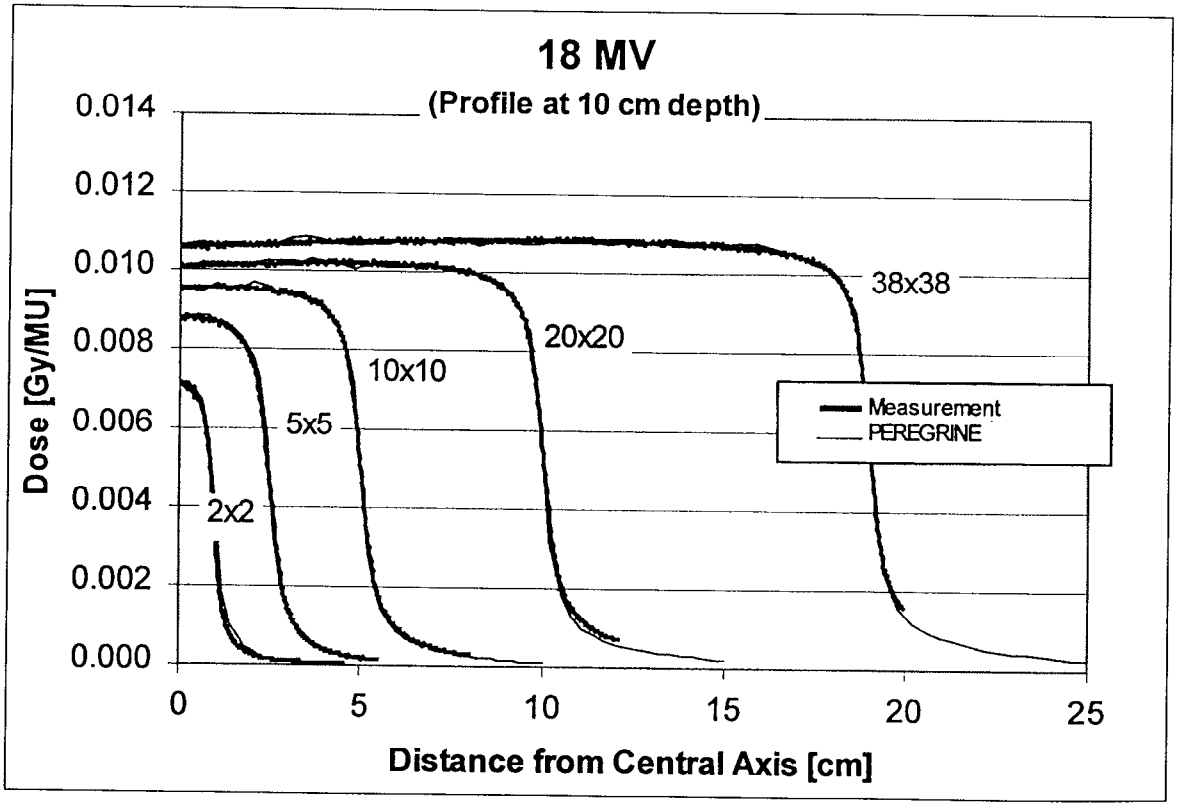

Evidence regarding dosimetric accuracy resulting from PEREGRINE's transport of particles through beam modifiers is demonstrated in Table 3, and Figures 4-6.

Figure 4 demonstrates the agreement between dose profiles resulting from at 20x20 cm field modified by three types of blocks: a half-beam block, a half-beam partial-transmission block, and a quarter-beam block. All blocks are positioned (and simulated) on a standard Lucite tray. By focussing on measurements at-depth, we demonstrate the effects of both photon transport through the block and photon transport in the water phantom. For each case, the open field portion of the beam is about the same. However, the partial-transmission block shows less of a fall-off near the block edge than does the standard half-beam block. Presumably, this is caused by more phantom scatter in the blocked region, which serves as a source to boost the dose near the central axis.

The wedge profiles shown in Figure 5 further demonstrate the accuracy of PEREGRINE's methods for transporting photons through the beam delivery system. Because each wedge has a constantly-changing thickness, their resulting dose distributions serve as an excellent test of photon transport though high-atomic-number media. The wedges measured and modeled here are composed of steel.

Comparison with multileaf collimator measurements (Figure 6) demonstrates how well Monte Carlo simulation predicts the dose resulting from a varying-resolution beam modifier. Leaves are positioned to simulate 4-cm, 2-cm, and 1-cm (single-leaf) line-pairs of open-blocked field incident on the phantom. It is evident that phantom scatter does not play a major role in changing the peak-to-valley ratio, even at greater profile depths.

Table 3. Beam modifier comparisons

Description	Data type	6 MV			18 MV			Detector
		Location	Accuracy	Position	Location	Accuracy	Position	
20x20 w/Half-Beam Block	DepthDose	at X=5 cm	0.38 %	N/A	at X=5 cm	0.40 %	N/A	IC-10
	XProfile	depth=5cm	0.57 %	0.65 mm	depth=10cm	0.65 %	0.59 mm	IC-10
	XProfile	depth=10cm	0.57 %	0.55 mm	depth=20cm	0.47 %	0.63 mm	IC-10
	XProfile	depth=20cm	0.43 %	0.90 mm	depth=30cm	0.41 %	0.81 mm	IC-10
20x20, Partial Transmission Half-Beam Block	DepthDose	at Y= -5 cm	0.54 %	N/A	at X= -5 cm	0.72 %	N/A	IC-10
	YProfile	depth=5cm	0.60 %	1.40 mm	depth=10cm	0.48 %	1.63 mm	IC-10
	YProfile	depth=10cm	0.72 %	1.38 mm	depth=20cm	0.37 %	1.22 mm	IC-10
	YProfile	depth=20cm	0.43 %	1.01 mm	depth=30cm	0.46 %	1.22 mm	IC-10
20x20, Quarter-Beam Block	DepthDose				central axis	0.39 %	N/A	IC-10
	XProfile	depth=5cm	0.54 %	0.78 mm	depth=10cm	0.45 %	0.90 mm	IC-10
	XProfile				depth=20cm	0.40 %	1.36 mm	IC-10
	XProfile	depth=20cm	0.47 %	1.42 mm	depth=30cm	0.38 %	1.34 mm	IC-10
20x20 Central 2x8 Block	DepthDose	at X=5 cm	0.40 %	N/A	at X=5 cm	0.41 %	N/A	IC-10
	XProfile	depth=5cm	1.02 %	1.01 mm	depth=10cm	0.68 %	0.65 mm	IC-10
	XProfile	depth=10cm	0.62 %	1.00 mm	depth=20cm	0.36 %	0.73 mm	IC-10
	XProfile	depth=20cm	0.31 %	0.94 mm	depth=30cm	0.31 %	0.75 mm	IC-10
10x10 Blocked to 5x5	DepthDose	central axis	0.99 %	N/A	central axis	0.48 %	N/A	IC-10
	XProfile	depth=5cm	1.42 %	1.18 mm	depth=10cm	1.06 %	1.34 mm	IC-10
	XProfile	depth=10cm	0.82 %	1.42 mm	depth=20cm	0.52 %	1.13 mm	IC-10
	XProfile	depth=20cm	0.64 %	1.20 mm	depth=30cm	0.36 %	1.34 mm	IC-10
5x5 4 cm Stereotactic Cone	DepthDose	central axis	0.89 %	N/A	central axis	0.61 %	N/A	IC-10
	XProfile	depth=5cm	1.71 %	1.41 mm	depth=10cm	1.22 %	1.05 mm	IC-10
	XProfile	depth=10cm	0.99 %	1.23 mm	depth=20cm	0.52 %	1.13 mm	IC-10
	XProfile	depth=20cm	0.48 %	1.35 mm	depth=30cm	0.28 %	1.15 mm	IC-10
20x40 15 Degree Steel Wedge	DepthDose	central axis	0.43 %	N/A	central axis	0.87 %	N/A	IC-10
	XProfile	depth=5cm	0.62 %	0.62 mm	depth=10cm	1.39 %	0.64 mm	IC-10
	XProfile	depth=10cm	0.65 %	0.65 mm	depth=20cm	0.64 %	0.62 mm	IC-10
	XProfile	depth=20cm	0.38 %	0.61 mm	depth=30cm	0.49 %	0.68 mm	IC-10
20x40 45 Degree Steel Wedge	DepthDose	central axis	0.71 %	N/A	central axis	0.32 %	N/A	IC-10
	XProfile	depth=5cm	0.95 %	0.51 mm	depth=10cm	0.52 %	0.54 mm	IC-10
	XProfile	depth=10cm	0.75 %	0.61 mm	depth=20cm	0.35 %	0.57 mm	IC-10
	XProfile	depth=20cm	0.39 %	0.62 mm	depth=30cm	0.37 %	0.56 mm	IC-10
15x40 60 Degree Steel Wedge	DepthDose	central axis	1.09 %	N/A	central axis	0.79 %	N/A	IC-10
	XProfile	depth=5cm	1.17 %	0.40 mm	depth=10cm	0.60 %	0.44 mm	IC-10
	XProfile	depth=10cm	0.94 %	0.32 mm	depth=20cm	0.41 %	0.32 mm	IC-10
	XProfile	depth=20cm	0.74 %	0.32 mm	depth=30cm	0.44 %	0.32 mm	IC-10
20x20 Brass Step Compensator	DepthDose	central axis	0.42 %	N/A	central axis	0.45 %	N/A	IC-10
	XProfile	depth=5cm	0.75 %	0.63 mm	depth=10cm	0.58 %	0.63 mm	IC-10
	XProfile	depth=10cm	0.60 %	0.66 mm	depth=20cm	0.53 %	0.69 mm	IC-10
	XProfile	depth=20cm	0.36 %	0.98 mm	depth=30cm	0.37 %	0.75 mm	IC-10

Figure 4. Dose profiles for half beam block, 50% transmission half beam block, and quarter beam block.

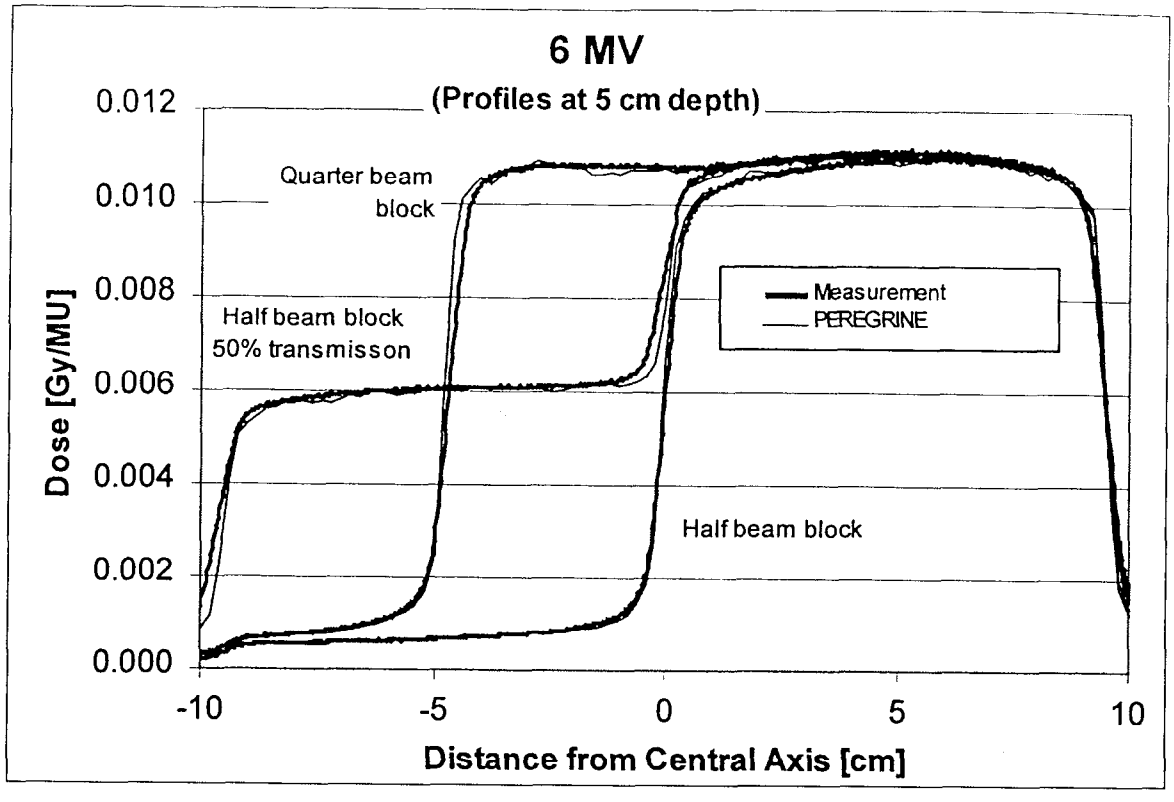

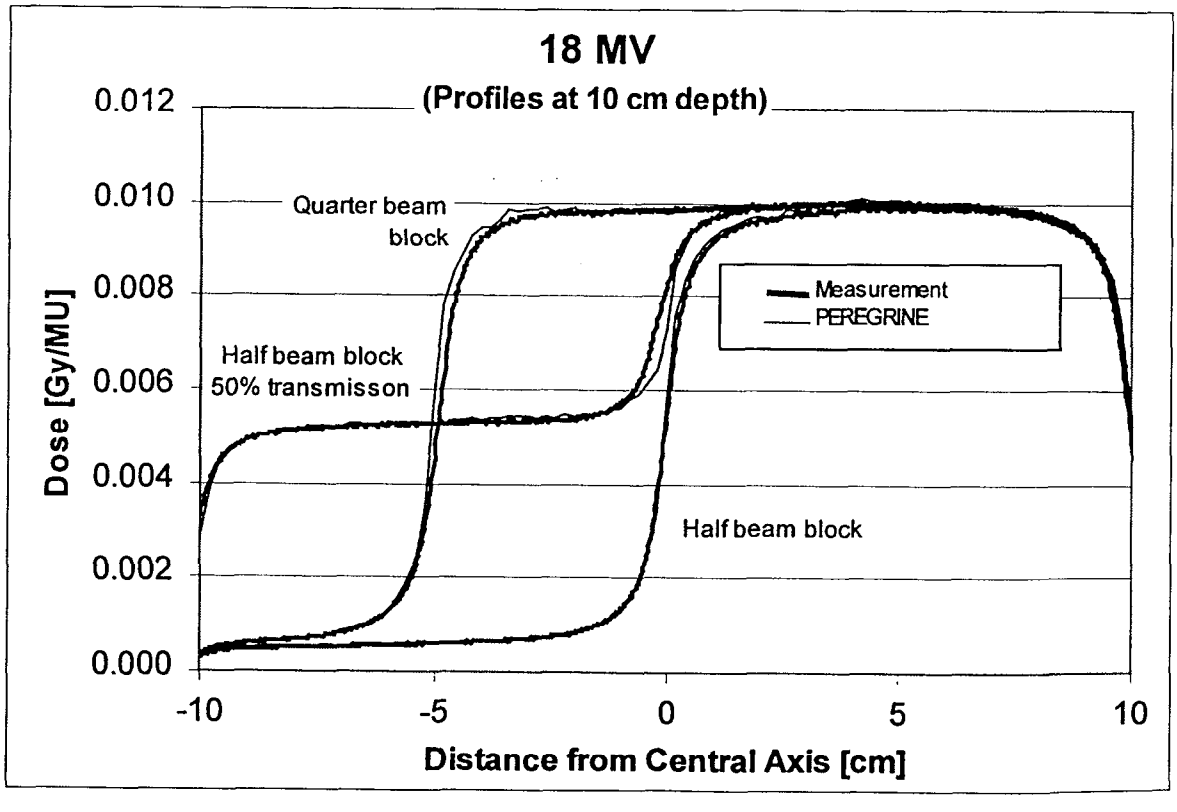

Figure 5. Dose profiles for 15, 45, and 60 degree wedges .

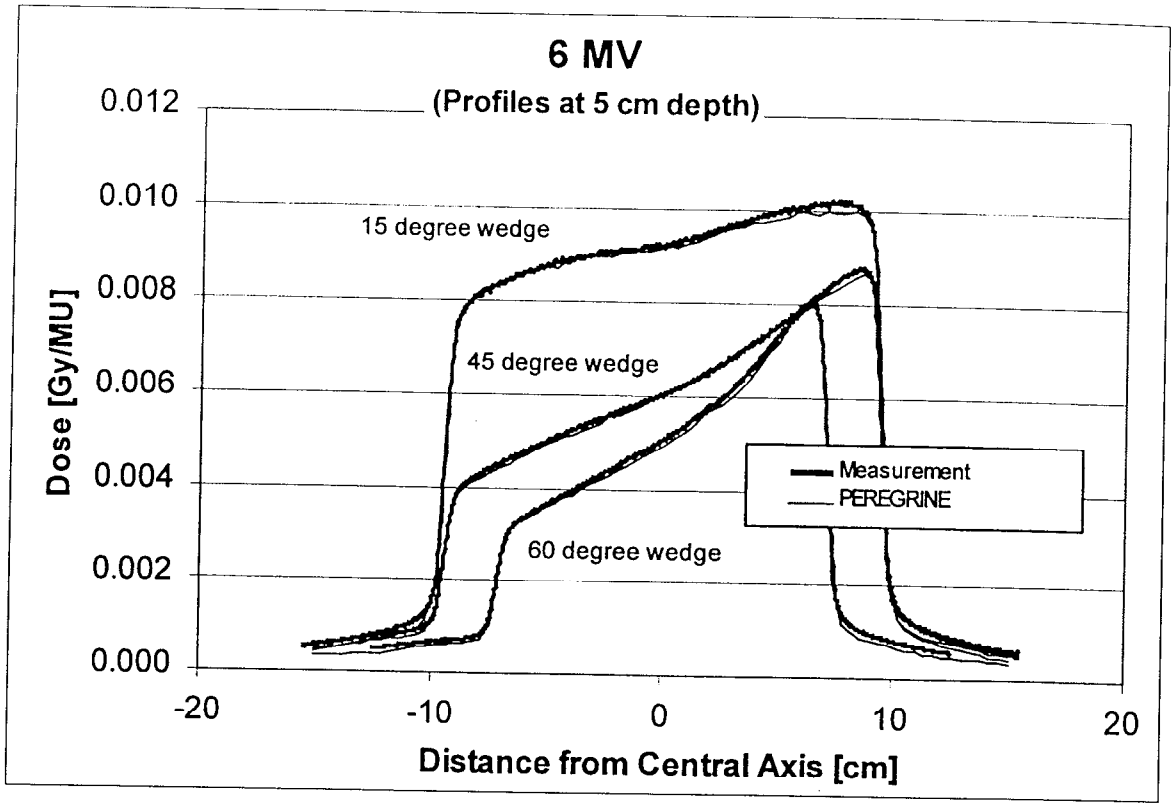

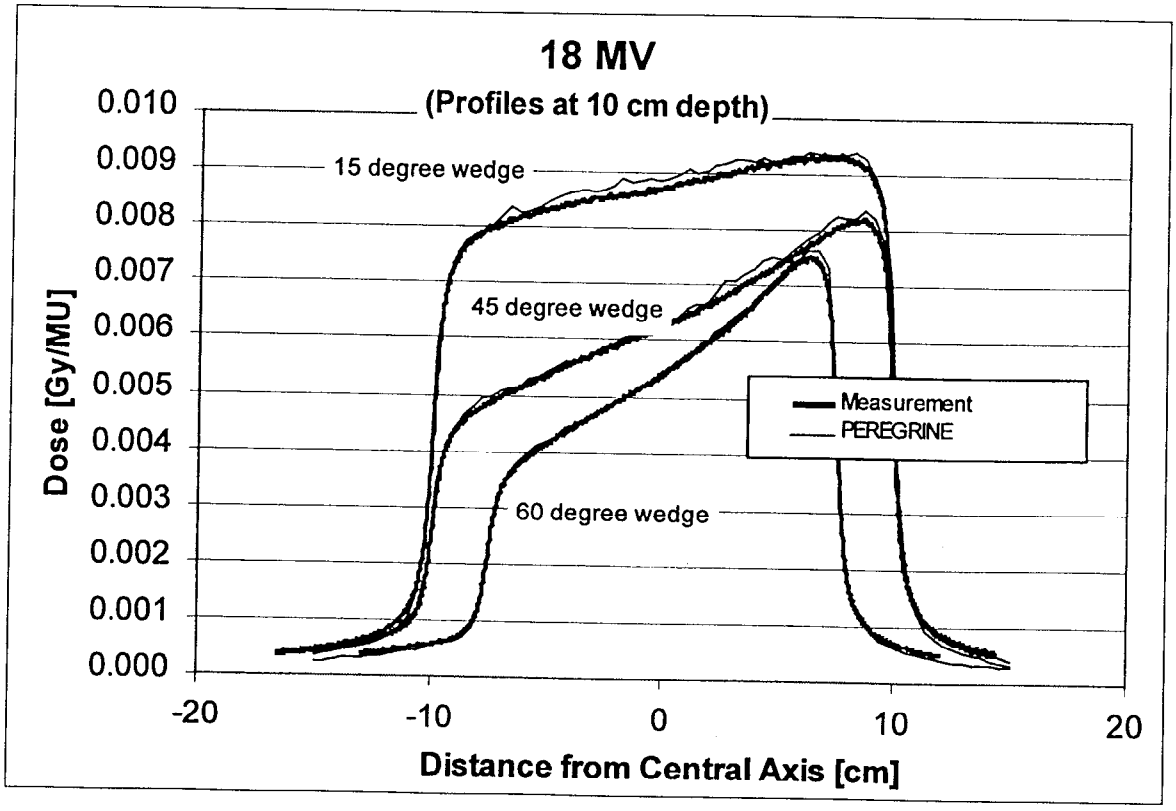

Figure 6. Dose profiles for multileaf collimators.

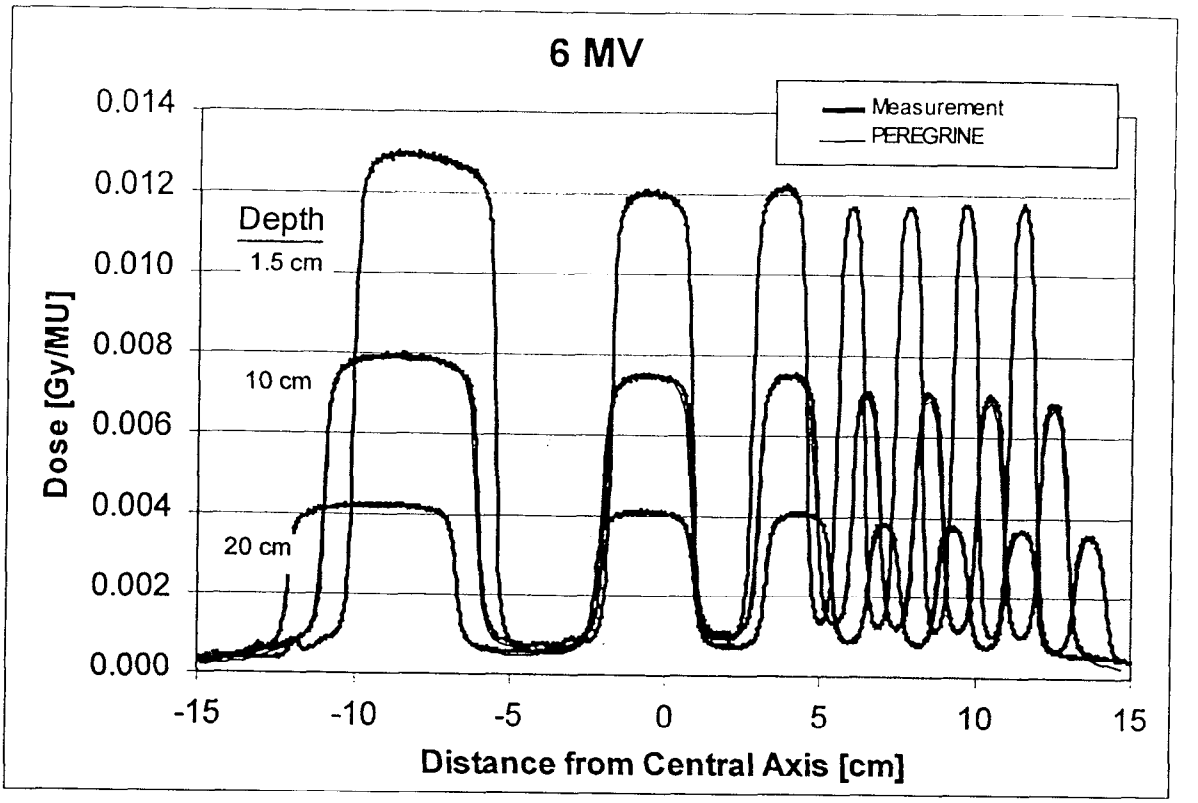

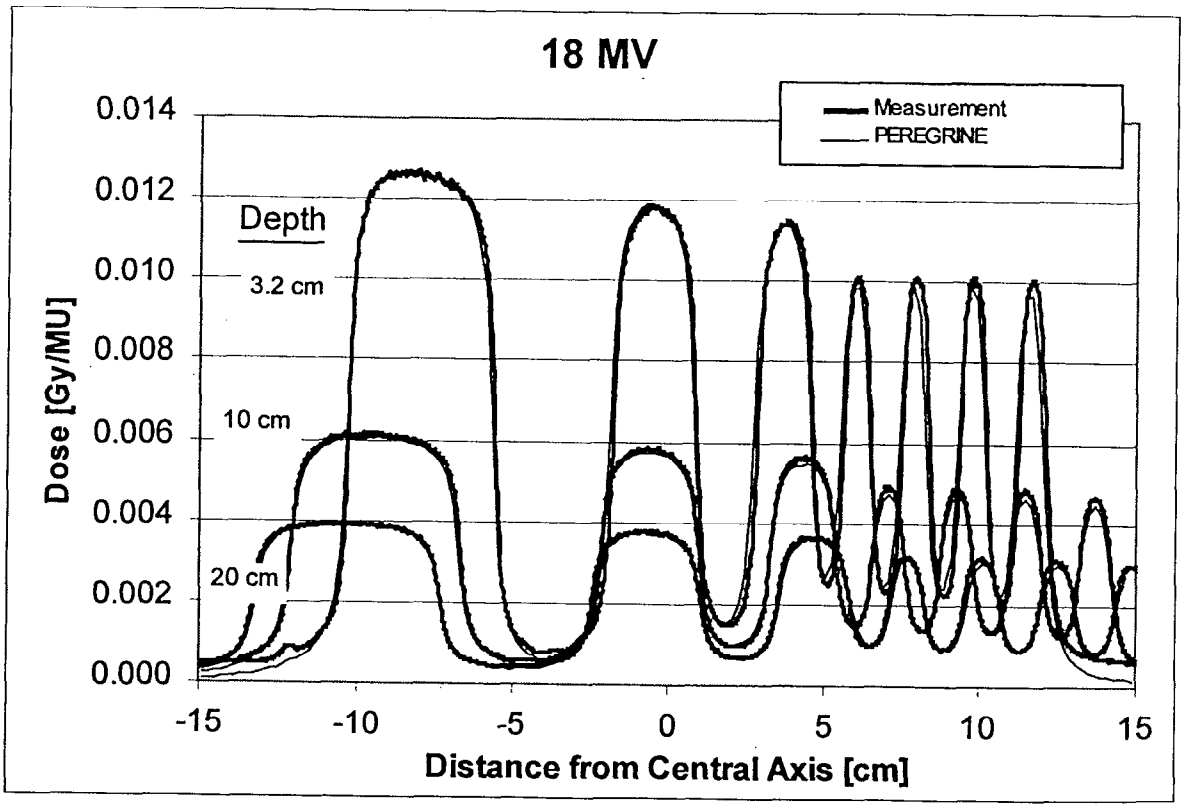

Measurement comparisons for open and modified fields calculations demonstrate the dosimetric accuracy resulting from PEREGRINE's transport of particles through both the beam delivery system and a simple water phantom. Table 4, accompanied by Figures 7-9, demonstrates the accuracy of PEREGRINE's photon and electron transport algorithms in accounting for irregular surfaces and heterogeneities in the patient. Agreement in areas greater than one electron range from the heterogeneous feature demonstrate the accuracy of PEREGRINE's photon transport algorithms, while agreement in areas near the heterogeneous surface demonstrate the accuracy of PEREGRINE's electron transport algorithms.

Figure 7 shows dose profile comparisons for a 20x20-cm beam incident on a water phantom with a 2-cm step positioned so that its edge is on the central axis of the beam. The 5-cm-depth profiles demonstrate the accuracy of PEREGRINE™ transport algorithms in photon scatter and attenuation in the phantom, while the 1-cm-depth profiles, which are in the buildup region for the no-step portion of the phantom, also demonstrate the accuracy of PEREGRINE's electron transport. This effect is seen in two ways. First, calculations and measurements at points distant from the step edge demonstrate the accuracy of electron transport in the phantom, plus the effects of contaminant electrons produced in the accelerator head and air column. These effects are particularly striking for the 18 MV case. Second, calculations and measurements near the step edge demonstrate the accuracy of electron transport near a complex, discontinuous surface. For 6 MV, transport of electrons from the step edge to the no-step side of the phantom and vice-versa result in a low-peak high-peak phenomena. For 18 MV, this same effect results in a kink in the dose fall-off as the ion chamber enters the region of non-electronic equilibrium.

Figure 8 demonstrates PEREGRINE's agreement with diode beam-profile measurements for a water phantom with 2-cm-thick air and steel heterogeneities, located at a depth 3 cm below the phantom surface and extending through half the radiation beam. The photon beam was a 20x8-cm 6- and 18-MV open fields. The excellent agreement for the first profile below the heterogeneity is particularly important as it depends on both accurate photon and electron transport. This comparison demonstrates PEREGRINE's prediction of the attenuating effects of each heterogeneous slab as well as its effects in areas of electron disequilibrium near its edges.

Table 4. Heterogeneity comparisons

Description	Data type	6 MV			18 MV			Detector
		Location	Accuracy	Position	Location	Accuracy	Position	
10x20 Lucite Step	XProfile	depth=7cm	0.58 %	0.59 mm	depth=5cm	0.50 %	0.45 mm	IC-10
	XProfile	depth=12cm	0.56 %	0.59 mm	depth=12cm	0.49 %	0.40 mm	IC-10
	XProfile	depth=22cm	0.46 %	1.23 mm	depth=22cm	0.49 %	0.42 mm	IC-10
10x20 3.5 cm Lucite Cylinder	XProfile	depth=9cm	0.98 %	0.58 mm	depth=7cm	0.99 %	0.46 mm	IC-10
	XProfile	depth=14cm	0.69 %	0.60 mm	depth=14cm	0.75 %	0.45 mm	IC-10
	XProfile	depth=24cm	0.40 %	0.46 mm	depth=24cm	0.47 %	0.60 mm	IC-10
10x20 7.5 cm Lucite Cylinder	XProfile	depth=13cm	0.79 %	1.14 mm	depth=11cm	1.03 %	0.48 mm	IC-10
	XProfile	depth=18cm	0.56 %	0.99 mm	depth=18cm	0.62 %	0.49 mm	IC-10
	XProfile	depth=28cm	0.32 %	1.36 mm	depth=20cm	0.38 %	0.53 mm	IC-10
20x8 Air Half-Slab	DepthDose	at X=5 cm	0.64 %	N/A	at X=5 cm	0.80 %	N/A	Markus Chamber
	DepthDose	at X= -5 cm	0.63 %	N/A	at X= -5 cm	0.53 %	N/A	Markus Chamber
	XProfile	depth=7cm	1.24 %	0.58 mm	depth=7cm	0.62 %	0.88 mm	Diode
	XProfile	depth=11cm	0.83 %	0.65 mm	depth=11cm	1.03 %	1.01 mm	Diode
	XProfile	depth=16cm	0.51 %	0.82 mm	depth=16cm	0.60 %	0.65 mm	Diode
	XProfile	depth=21cm	0.55 %	0.64 mm	depth=26cm	0.37 %	0.54 mm	Diode
20x8 Lung Half-Slab	DepthDose	at X=5 cm	0.57 %	N/A	at X=5 cm	0.47 %	N/A	Markus Chamber
	DepthDose	at X= -5 cm	0.38 %	N/A	at X= -5 cm	0.39 %	N/A	Markus Chamber
	XProfile	depth=7cm	0.60 %	0.75 mm	depth=7cm	0.83 %	0.59 mm	Diode
	XProfile	depth=11cm	0.57 %	0.70 mm	depth=11cm	0.49 %	0.66 mm	Diode
	XProfile	depth=16cm	0.47 %	0.68 mm	depth=16cm	0.42 %	0.60 mm	Diode
	XProfile	depth=21cm	0.45 %	0.81 mm	depth=26cm	0.53 %	0.61 mm	Diode
20x8 Bone Half-Slab	DepthDose	at X=5 cm	0.69 %	N/A	at X=5 cm	0.51 %	N/A	Markus Chamber
	DepthDose	at X= -5 cm	0.32 %	N/A	at X= -5 cm	0.39 %	N/A	Markus Chamber
	XProfile	depth=7cm	1.11 %	1.31 mm	depth=7cm	0.81 %	0.67 mm	Diode
	XProfile	depth=11cm	0.70 %	1.39 mm	depth=11cm	0.85 %	0.71 mm	Diode
	XProfile	depth=16cm	0.91 %	0.44 mm	depth=16cm	0.68 %	0.60 mm	Diode
	XProfile	depth=21cm	0.49 %	0.84 mm	depth=26cm	0.58 %	0.62 mm	Diode
20x8 Steel Half-Slab	DepthDose	at X=5 cm	0.80 %	N/A	at X=5 cm	0.51 %	N/A	Markus Chamber
	DepthDose	at X= -5 cm	0.42 %	N/A	at X= -5 cm	0.44 %	N/A	Markus Chamber
	XProfile	depth=7cm	1.08 %	0.30 mm	depth=7cm	0.78 %	0.62 mm	Diode
	XProfile	depth=11cm	0.68 %	0.75 mm	depth=11cm	0.65 %	0.71 mm	Diode
	XProfile	depth=16cm	0.65 %	0.37 mm	depth=16cm	0.52 %	0.58 mm	Diode
	XProfile	depth=21cm	0.59 %	0.74 mm	depth=26cm	0.33 %	0.51 mm	Diode
20x26 MLC comb pattern	DepthDose	at Y=0	0.83 %	N/A	at Y=0	0.57 %	N/A	IC-10
	DepthDose	at Y= -8 cm	0.30 %	N/A	at Y= -8 cm	0.82 %	N/A	IC-10
	YProfile	depth=5cm	1.42 %	0.46 mm	depth=10cm	0.60 %	0.38 mm	Diode
	YProfile	depth=10cm	0.94 %	0.55 mm	depth=20cm	0.77 %	0.32 mm	Diode
	YProfile	depth=20cm	0.57 %	0.26 mm	depth=30cm	0.52 %	0.62 mm	Diode

Figure 7. Dose profiles in a phantom with a 2 cm lucite step.

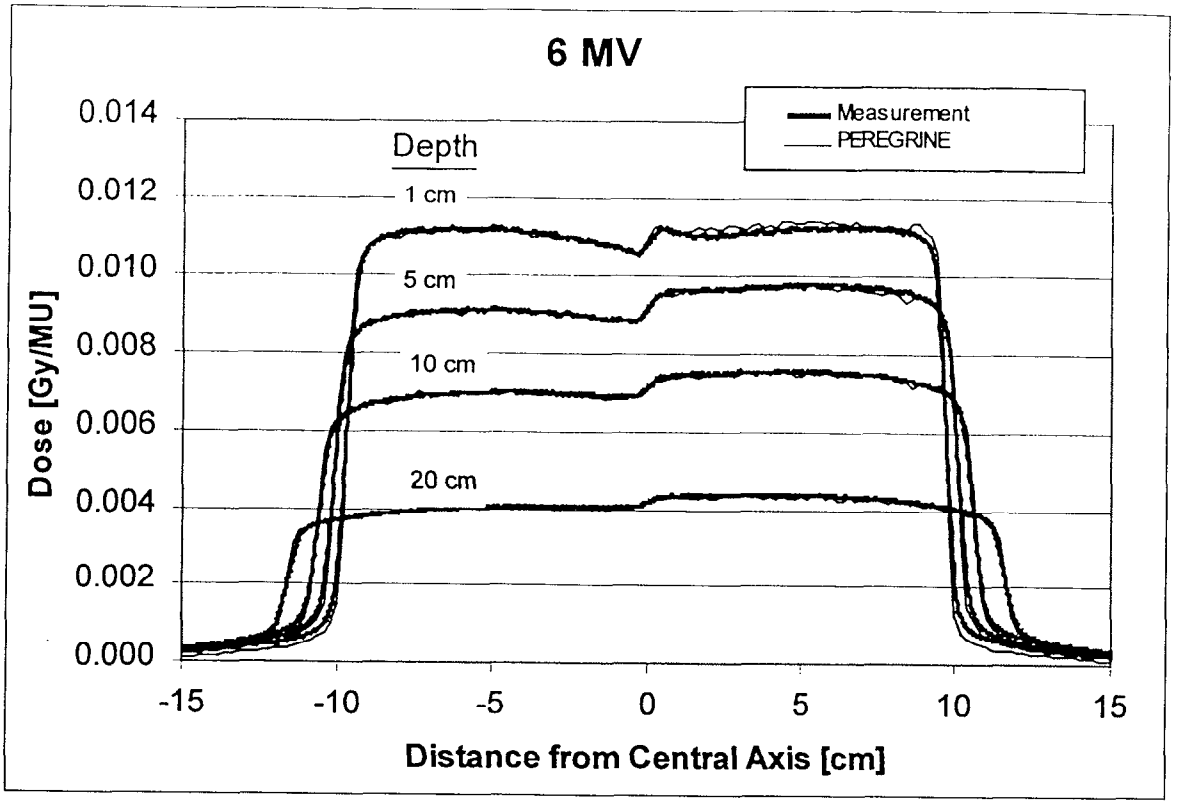

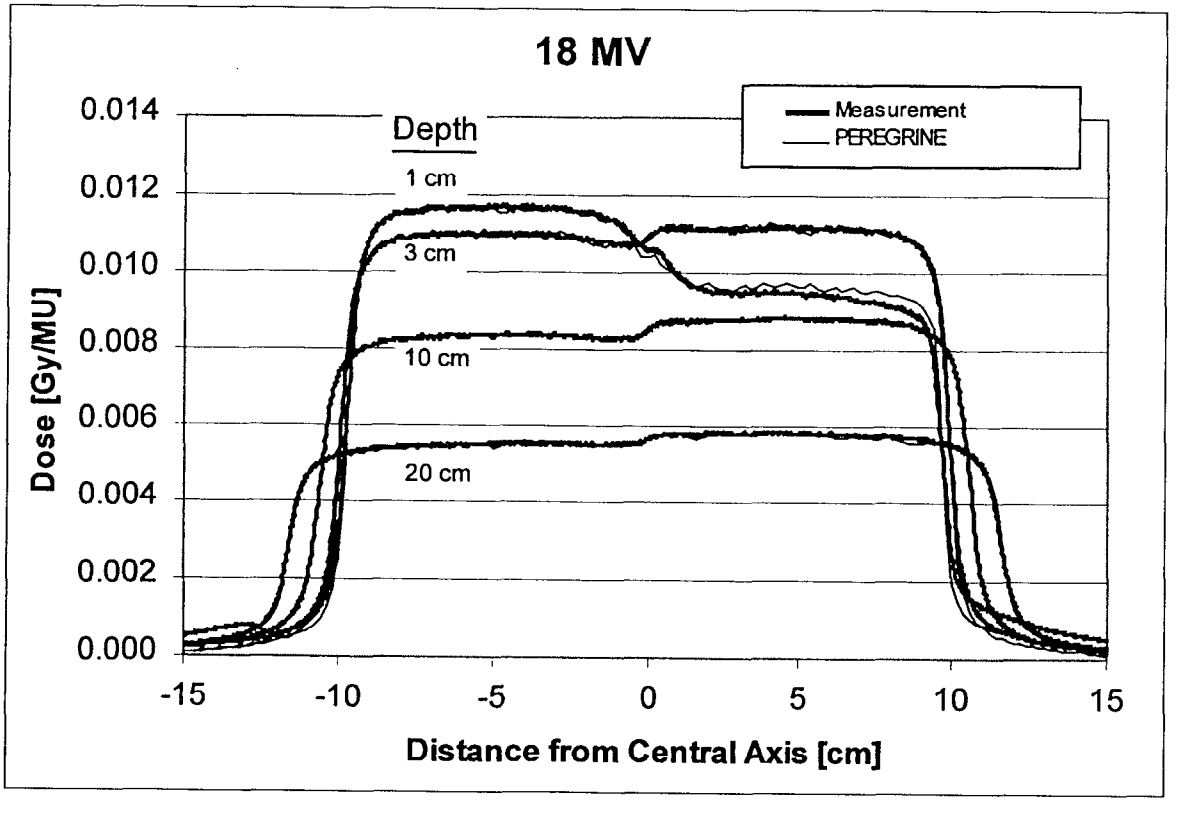

Figure 8. Dose profiles in a phantom with "thick air" and steel heterogeneities.

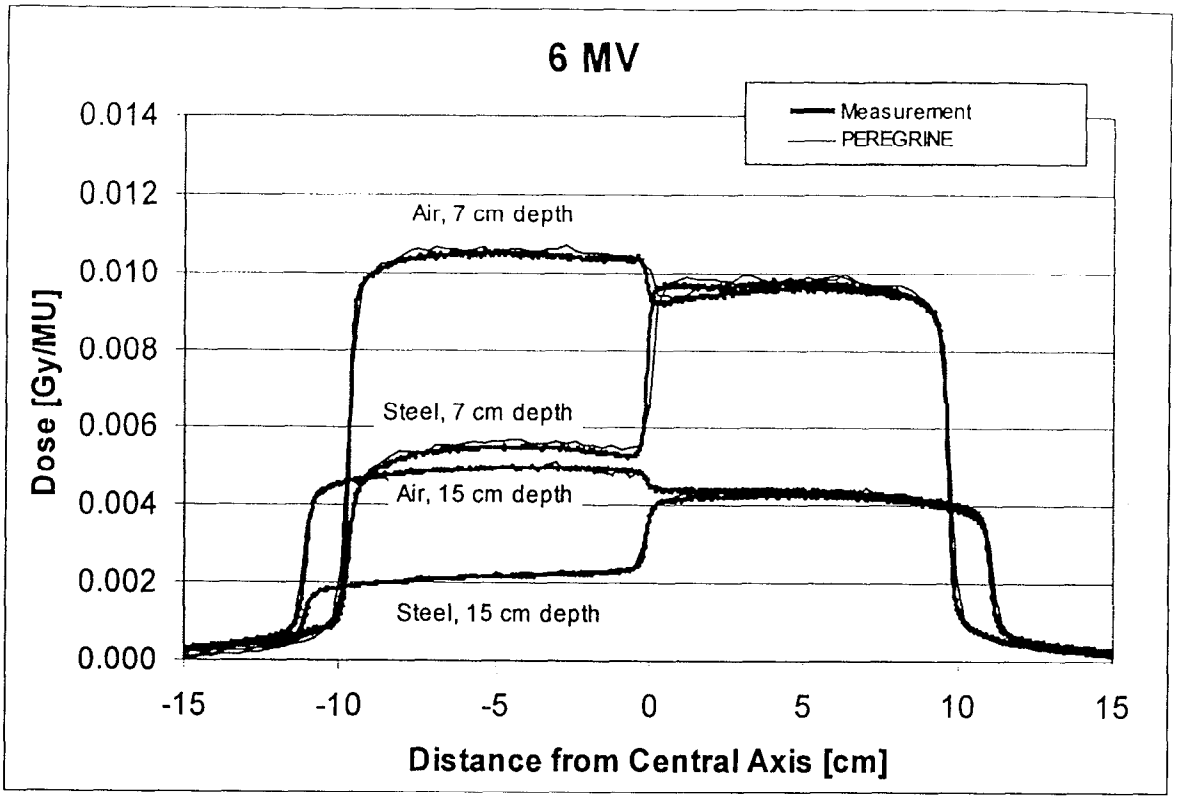

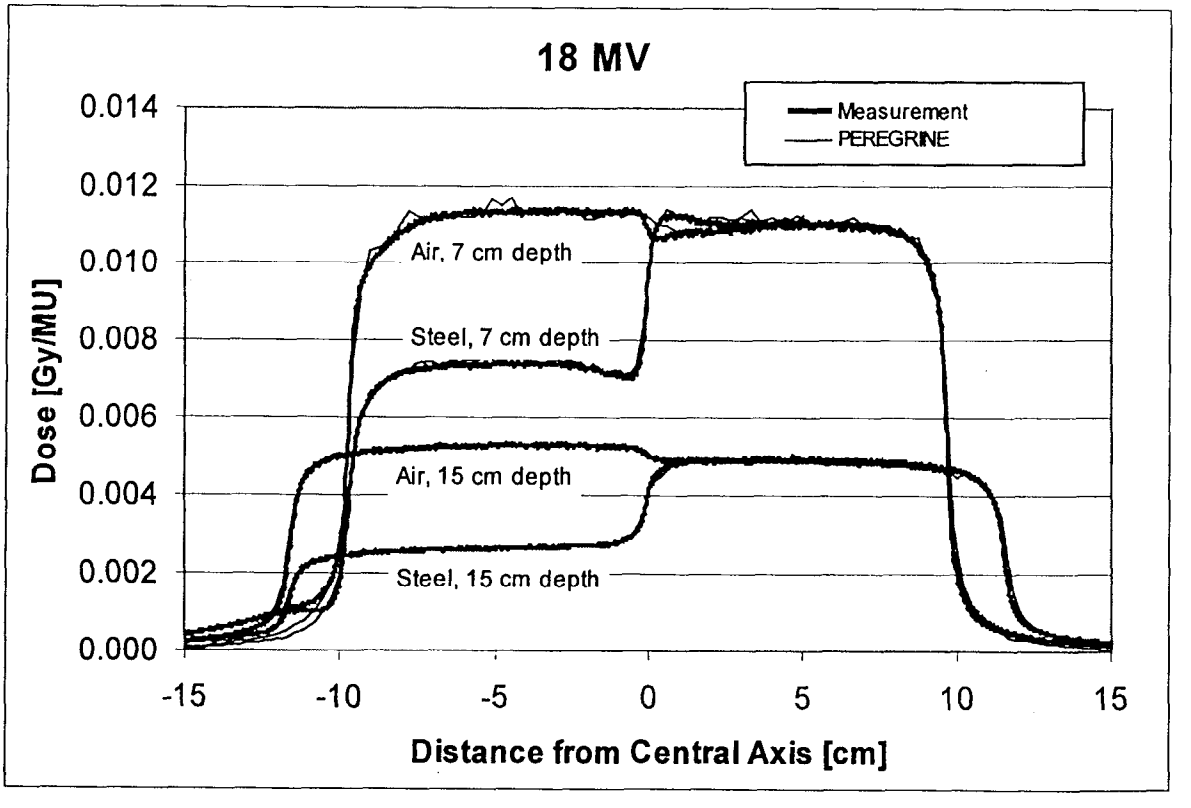

Conclusions

The success of radiation therapy requires three critically linked components: patient evaluation, treatment planning, and treatment delivery. In the last several decades, technology for patient evaluation and treatment delivery have improved dramatically, providing an array of imaging and treatment delivery devices that has so far outmatched the radiation therapy field's ability to fully utilize them. However, full realization of the benefits of these advances requires sophisticated, accurate treatment planning.

Monte Carlo dose calculations are the gold standard for dose calculations. They accurately compute dose in a wide variety of radiation therapy conditions including those conditions we have tested here. By taking advantage of recent advances in computer technology, combined with state-of-the-art Monte Carlo transport algorithms, PEREGRINE™ performs high-resolution Monte Carlo radiation treatment planning calculations in times compatible with use in a radiation therapy clinic, using low-cost commodity hardware. Because of its speed and ease of use, PEREGRINE™ has the capacity to bring Monte Carlo radiation transport calculations to the clinical RTP desktop environment.

Results of the PEREGRINE™ dosimetric validation suite demonstrate PEREGRINE's accuracy for a wide range of beam and patient configurations, stressing all important Monte Carlo transport algorithms and system characteristics. PEREGRINE™ agrees with measurements to within <2% in regions of low dose gradient, and with a dose-positional uncertainty of <2 mm in regions of high dose gradient. Our results demonstrate that PEREGRINE™ can deliver dose calculations with uncertainties that are consistent with the ICRU 42 recommendations and significantly smaller that the experience-based criteria given in TG 53.

Employing PEREGRINE™ 3D Monte Carlo dose calculations for widespread clinical use will improve the accuracy of radiation therapy dose calculations for every patient. This will facilitate more accurate clinical trials and reliable implementation of their results throughout the medical community, provide more accurate estimates of required doses for tumor control and normal tissue tolerance, and aid in the advancement of the field of radiation oncology.

---

1. R. Mohan, "Dose Calculations for Radiation Treatment Planning," in T. M. Jenkins, W. R. Nelson, and A. Rindi, eds., Monte Carlo Transport of Electrons and Photons, 549-471 (1988).

2. D. W. O. Rogers and A. F. Bielajew, "Monte Carlo techniques of electron and photon transport for radiation dosimetry," in *The Dosimetry of Ionizing Radiation*, Vol. III, edited by K. R. Kase, B. E. Bjarngard, and R. H. Attix (academic, New York pp.427-539 (1990).

3. T. R. Mackie, "Applications of the Monte Carlo method in radiotherapy," in *The Dosimetry of Ionizing Radiation*, Vol. III, edited by K. R. Kase, B. E. Bjarngard, and R. H. Attix, Academic, New York (1990), pp.541-620.

4. L. Wang, C. S. Chui, and M. Lovelock, "A patient-specific Monte Carlo dose-calculation method for photon beams," Med. Phys. 25(6) pp. 867-878 (1998).

5. J. J. DeMarco, T. D. Solberg, and J. Bl Smathers, "A CT-based Monte Carlo simulation tool for dosimetry planning and analysis," Med. Phys. 25(1), 1-10 (1998).

6. C.-M. Ma, E. Mok, A. Kapur, T. Pawlicki, D. Findley, S. Brain, K. Forster, and A. L. Boyer "Clinical implementation of a Monte Carlo treatment planning system" Med. Phys. 26:8 2133-2143 (1999).

7. C. L. Hartmann Siantar, P. M. Bergstrom, W. P. Chandler, L. Chase, L. J. Cox, T, et. al., *XIIth International Conference on the use of Computers in Radiation Therapy*, p. 19-22, Medical Physics Publishing, Madison, Wisconsin,1997.

8. C. L. Hartmann Siantar, P. M. Bergstrom, W. P. Chandler, L. J. Cox, P. Daly, D. Garrett, R. K. House, E. I. Moses, R. W. Patterson, and E. Schach von Wittenau, Fast Monte Carlo for Radiotherapy - the PEREGRINE™ Project, Proceedings of the 1998 ANS Radiation Protection and Shielding Division Topical Conference: Technologies for the New Century, April 19-23, 1998, Nashville, TN.

9. C. L. Hartmann Siantar, P. M. Bergstrom, L. J. Cox, T. P. Daly, D. H. Fujino, M. Descalle, D. Garrett, B. Guidry, R. K. House, D. Jong, D. K. Knapp, S. H. May, E. I. Moses, R. W. Patterson, C. Powell, D. M. Williams, A. E. Schach von Wittenenau, R. S. Walling, J. A. White, N. Albright, L. Verhey, D. Wieczorek and M. C. Schell, "Implementation of the PEREGRINE™ Monte Carlo dose calculation system for photon beam therapy," submitted to Phys. Med. Biol.

10. ICRU Report 42 "Use of computers in external beam radiotherapy procedures with high-energy photons and electrons" ICRU Publications Bethesda MD (1988).

11. B. A. Fraass, K. Doppke, M. Hunt, G. J. Kutcher, G. Starkschall, R. Stern, J. van Dyk, "Quality assurance for clinical radiotherapy treatment planning: Report of the radiation therapy committee task group #53", Med. Phys. 25(10) p. 57 (1997).

12. J Van Dyk, R Barnett J Cygler, P Shragge, "Commissioning and quality assurance of treatment planning computers," Int J Rad Oncol Biol Phys 26: 261-273 (1993).

13. B. A. Fraass, "Quality assurance for 3D treatment planning in Teletherapy: Present and Future, Proceedings of the 1996" Summer School American Association of Physicists in Medicine Advanced Medical Publishing p. 253-318 (1996).

14. A. E. Schach von Wittenau, L. J. Cox, P. M. Bergstrom, W. P. Chandler, C. L. Hartmann Siantar, and R. Mohan "Correlated histogram representation of Monte Carlo derived medical accelerator photon-output phase space," *Med. Phys.* **26**:7 1196-1211 (1999).

15. A. Duzenli, B. McClean and C. Field, "Backscatter into the beam monitor chamber: Implications for dosimetry of asymmetric collimators," Med. Phys. 20:2, Pt. 1 363-367 (1993).

16. J. Cunningham "Quality assurance in dosimetry and treatment planning" Int J Rad Oncol Biol Phys 10: 105-109 (1983).